GeoAmericas2020
4th PAN AMERICAN CONFERENCE ON GEOSYNTHETICS
26-29 APRIL 2020 • RIO DE JANEIRO • BRAZIL

Shear band formation in uniformly graded, geotextile reinforced triaxial samples

D.H. Marx, Department of Civil, Architectural and Environmental Engineering, University of Texas at Austin, Austin, United States of America
J.G. Zornberg, Department of Civil, Architectural and Environmental Engineering, University of Texas at Austin, Austin, United States of America

ABSTRACT

Geotextile reinforced triaxial tests were done on fused quartz samples saturated with mineral oil. Due to the match in refractive indices of the quartz and the oil the mixture was transparent. By illuminating the samples with a red laser, it was possible to track particle movement within the samples and thus measure shear band formation. The scope of this study was limited to 2.9 mm uniform graded quartz, tested at only one confining stress (~190 kPa). The effect of the geotextile on the failure strength of the samples was less pronounced than expected. However, the geotextile did provide lateral restraint to the sample. In addition, the shear band did not extend through the geotextile and was limited to either halve of the soil. Furthermore, the location of the band of soil actively failing continuously changed throughout the test.

1. INTRODUCTION

Geosynthetics are commonly used to improve the strength and stiffness of soils. Several soil-geosynthetic interaction tests have been developed to simulate the various failure mechanisms of the soil-geosynthetic composites (Palmeira, 2009). One of the tests used to study the effect of geosynthetics on the strength of soil is a modified form of the conventional triaxial test. In this study geotextile reinforced fused quartz samples were tested in a conventional triaxial setup to investigate the effect of a geotextile inclusion on the shear strain distribution within the sample.

2. METHODOLOGY

A transparent granular media can be prepared by mixing fused quartz with oils with a similar refractive index (Ezzein & Bathurst, 2011). Due to the match in refractive indexes between the quartz and the oil light can pass through the media without refracting. Consequently, the media is transparent. When a laser is shined into the sample internal reflection of the particles results in the illumination of those particles. By capturing photos of the laser-illuminated particles it is possible to track the movement of the particles while subjected to an axial load.

For this study 2” diameter fused quartz samples were tested in a conventional triaxial load frame (see Figure 1a). The samples were constructed from a sieved, uniform graded (2.36 mm – 3.35 mm [#6 - #8]), fused quartz and saturated with a mixture of 52% Puretol 7 Special and 48% Paraflex HT4 manufactured by Petro-Canada (Peng & Zornberg, 2017). The large, uniform, particles were tested to ensure the optimal definition of those particles when illuminated by the laser.

The results of testing done on four representative samples are discussed in this paper. Two samples were unreinforced and two were reinforced mid-way with a disk of woven, polypropylene geotextile. The geotextile has a reported ultimate tensile strength of 70 kN/m of and apparent opening size of 0.6 mm. A photo of the reinforced sample during flushing is shown in Figure 1b. The bottom halve that has been saturated is transparent, while dry top is still opaque. As the latex membranes conventionally used for triaxial testing are not transparent, nor compatible with oil, purpose made membranes were manufactured from a medium-soft (40A on the durometer scale) silicone rubber. The same oils used for saturation was used to apply the confining stress to the sample.

The samples were tested at an effective stress of ~190 kPa after back pressure saturation to ~300 kPa. The load was applied at a rate of 6%/hour. Area correction (Head, 2014) and correction for membrane penetration (Frydman et al, 1973) was applied. A 450 mW red laser with a wavelength of 638 nm was use to illuminate the samples while digital images were captured with a Canon EOS 5DS R camera fitted with a 24-70 mm lens, as shown in Figure 1a. The only source of illumination of the sample was the red laser.

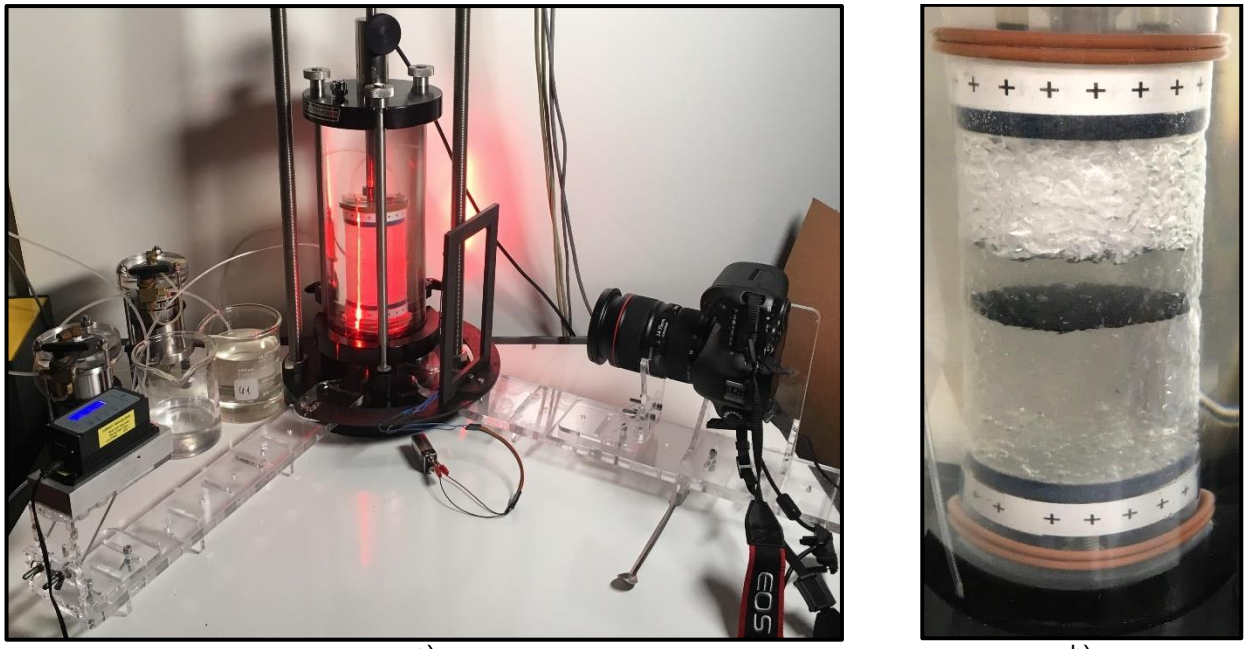

a) b)

Figure 1. Experimental setup a) triaxial cell, laser and camera b) reinforced sample during flushing.

Digital images were captured during the test at a rate of approximately one image per 0.02% axial strain in RAW format. As the sample was illuminated by red light only, the intensities from the red pixels were extracted from the Bayer mosaic stored in the RAW file. Subsequently, the equivalent red intensities at the location of the blue and green pixels were interpolated based on their respective distances from the red pixels. This matrix of interpolated red intensities was converted to a monochrome image. Refraction of the laser light from the sample and confining oil into the outside air, through the curved plexiglass cell, resulted in horizontal distortion of the sample. Correcting this distortion is non-trivial and was not done for these analyses as it has no influence on the mechanisms observed other than skewing the aspect ratio.

The displacement of particles between successive images was measured using the GeoPIV RG digital image correlation (DIC) software (Stanier et al, 2016). This software tracks the position of a unique patch of pixels in successive images of the test. Subsequently, the displacement of the particles can be calculated from the measured coordinates. Additional image processing was done to isolate the position of the geotextile in the sample during the test, as discussed in a subsequent section.

3. RESULTS AND DISCUSSION

The properties of the four samples after consolidation, as well as the peak friction angle and maximum angle of dilation calculated for the individual are summarized in Table 1. The corresponding stress-strain and volumetric strain-axial strain responses are shown in Figure 2a and Figure 3 respectively. The angle of dilation was calculated as $\sin\psi = -d\varepsilon_v/|d\varepsilon_q|$, where $d\varepsilon_q = 2(d\varepsilon_1 - d\varepsilon_3)/3$ (Li & Dafalias, 2000).

Table 1. Summary of samples tested.

Property	Unreinforced 1	Unreinforced 2	Reinforced 1	Reinforced 2
Void ratio	0.72	0.69	0.73	0.72
Dry density [g/cm³]	1.280	1.302	1.274	1.284
Confining stress [kPa]	189.8	188	188.5	174.7
Peak friction angle (Φ) [°]	41.3	41.0	42.2	46.7
Maximum angle of dilation (ψ) [°]	12.6	14.38	7.22	7.26

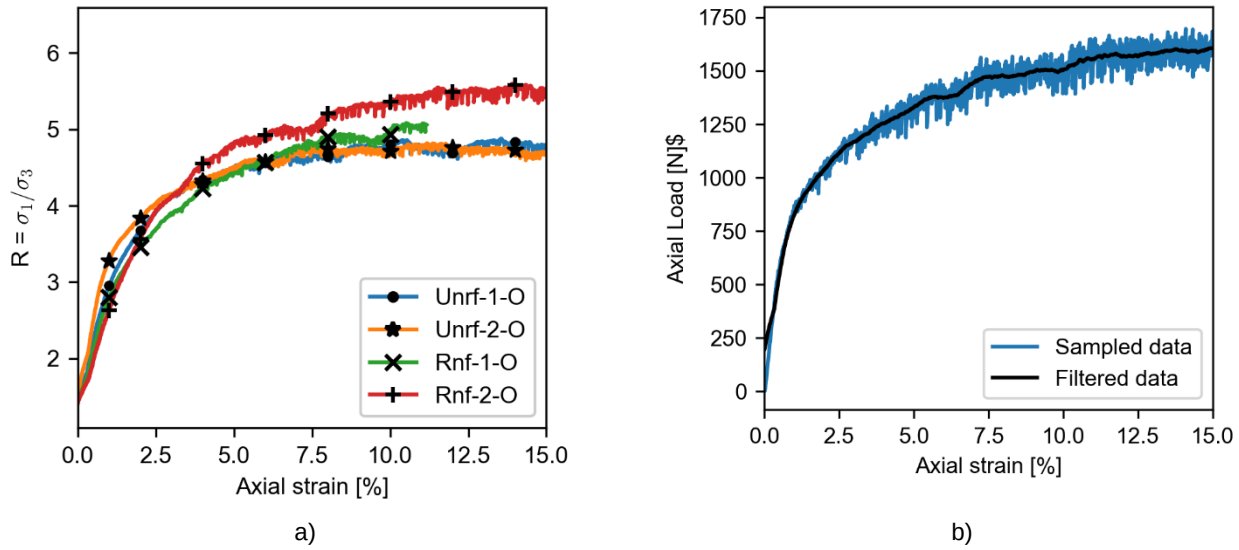

a) b)

Figure 2. Stress-strain response of the unreinforced and reinforced samples a) comparison of stress ratios and b) illustration of data filtering

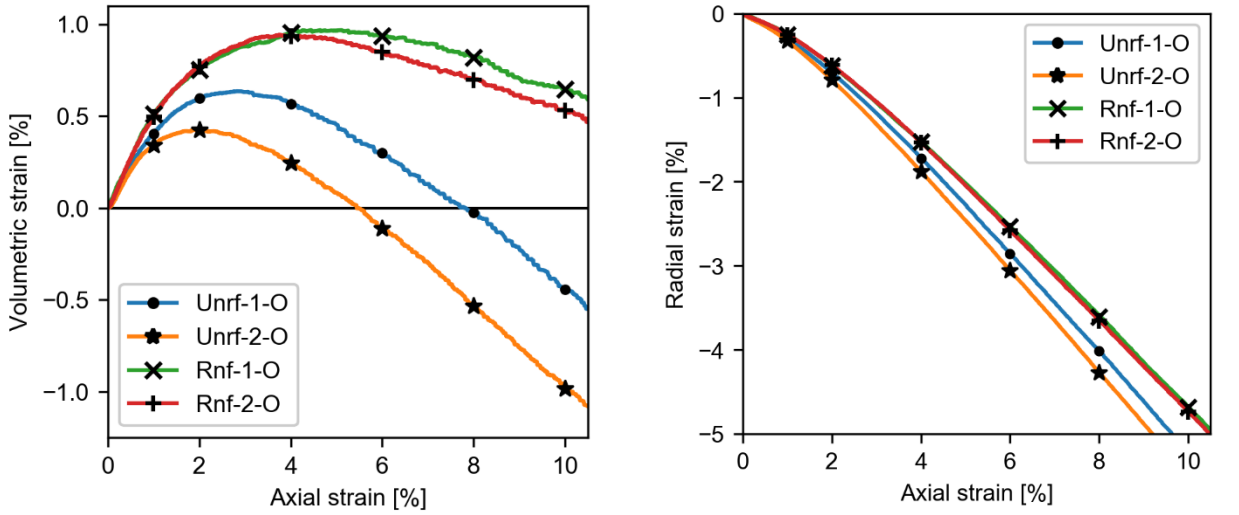

a) b)

Figure 3. Volumetric (a) and radial (b) strain response of the reinforced and unreinforced samples

Due to the “slip-stick” behavior of the lubricated fused quartz (Ezzein & Bathurst, 2011; Ozbay & Cabalar, 2016) the deviatoric stress oscillated severely while the sample was loaded (see Figure 2b) Consequently, a rolling average of the deviatoric stress was calculated for better visual comparison of the stress-strain responses. The peak of this rolling average was also used to calculate the peak friction angle. To further enable comparison of the results the peak stress ratio is presented (Figure 2a) to compensate for variations in the applied confining stress.

The two unreinforced samples plateaued at the same stress ratio with only a small difference in initial elastic stiffness due to different initial densities. For the reinforced samples the initial elastic response is the same with the curves diverging only at an axial strain of ~2.5%. The difference in strength is 4.5° if interpreted in terms of the Mohr-Coulomb friction angle. This difference in strength may result from the reinforcement effect or due to eccentricity of the second reinforced sample during testing.

The stress ratios of the reinforced and unreinforced samples were similar, suggesting that the reinforcing effect of the geotextile is not as pronounced as would be expected from literature (Haeri et al, 2000; Latha & Murthy, 2006; Goodarzi

& Shahnazari, 2019). However, the dilation angle of the unreinforced samples was greater than the reinforced, similar to the results reported by Haeri et al (2000). This behavior will be investigated in a subsequent section.

3.1 Volumetric response.

From the volumetric strain-axial strain response (see Figure 3a) both the unreinforced and reinforced sands have dilative tendencies. However, none of the samples exhibited significant strain softening, as typically expected from a dilative sample. Guo & Xu (2007) found that angular sand has a lesser tendency to strain soften due to the interplay between dilation and degraded interlock with increased axial strain in the sample. Furthermore, Amirpour Harehdasht (2017) found that strain softening tends to decrease as the confining pressure increased. Thus, the lack of strain softening is the consequence of the test design, i.e. coarse particles tested at a high confining stress (190 kPa).

The volumetric response of the two unreinforced samples was similar, and so was that of the two reinforced samples. After the initial contraction the reinforced samples experienced less dilation than the unreinforced, as reported in literature (Haeri et al, 2000). In addition, the reinforced samples strained less radially than the unreinforced samples (see Figure 3b). It can be shown that a sample of length *H* and one of length *H/2* (i.e. one bisected by a geotextile), subjected to the same axial strain level will have similar maximum radial strain. Consequently, the reduced radial strain experienced by the reinforced samples is not an artefact of the geometry of the test, but due to lateral restraint provided by the geotextile. The influence of geosynthetics on lateral restraint is of significance when the rutting performance of reinforced roads and deformation of reinforced soil is studied.

3.2 Shear band formation

The maximum shear strain on a plane in one of the unreinforced and one of the reinforced samples, at three axial strain levels, is shown in Figure 4. For both samples the shear strain does not follow any distinguishable pattern while the samples are in the elastic range ($\varepsilon_a = 1\%$). At 5% axial strain some shear strain concentration starts to form. However, it is only at 10% axial strain when clearly defined regions of concentrated shear strain can be identified. By 10% axial strain the stress-strain response of both samples has plateaued (see Figure 2a). For the unreinforced sample a significant strain concentration occurred spanning from the top right of the sample down to the bottom left. A secondary strain concentration bifurcates the main concentration from the top left corner. For the reinforced sample the strain concentrations are indistinct in the bottom half of the sample. However, in the top half of the sample the strain concentration reaches from the top right of the sample to the left side of the geotextile.

Histograms of the maximum, total shear strain distributions of all four samples are shown in Figure 5. Three of the four samples had similar shear strain distributions while the second unreinforced sample experienced slightly higher average shear strains. As the test progressed the average shear strain increased while the distributions remained fairly symmetric.

The shear bands visible in Figure 4 are the maximum cumulative shear strains through the sample and not active zone of failure. Strain distributions of incremental shear strain can assist in identifying the active shear bands in the samples. Consider the incremental strain distributions shown in Figure 6. Each incremental strain distribution was calculated over an increment of 0.5% axial strain. Successive distributions are shown from 8.5% to 10% strain. For both the unreinforced sample and the reinforced sample the orientation of the shear band changes between the increments under consideration. When these shear bands are accumulated it forms the shear strain distribution shown in Figure 4.

It appears that at a given time the applied stress is supported by a particular particle chain up to the point where that region becomes unstable and the load is shed to a different part of the sample. This process of shear bands forming, and degrading continues as the test progresses, resulting in a barrel-like sample at the end of the test. This behavior is accentuated for the samples under consideration that are uniformly graded with fairly large particles. It is postulated that for smaller particles similar behavior occurs. However, it is on a smaller scale and overall the sample behaves more as a continuum resulting in the typical well-defined failure planes. The identification of the shear bands was found to be highly depended on the axial strain under consideration, as well as the size of the increment over which the strain is calculated. As such none of the shear bands shown in Figure 6 can be considered the true active shear band in the sample, but rather the average of the shear bands that formed over the 0.5% increment of axial strain.

Finally, it can also be observed that for the reinforced samples the shear band was confined to either of the two halves of the sample. At no stage did the shear band bisect the geotextile. Thus, the two halves of the sample were loaded, and failed, independently.

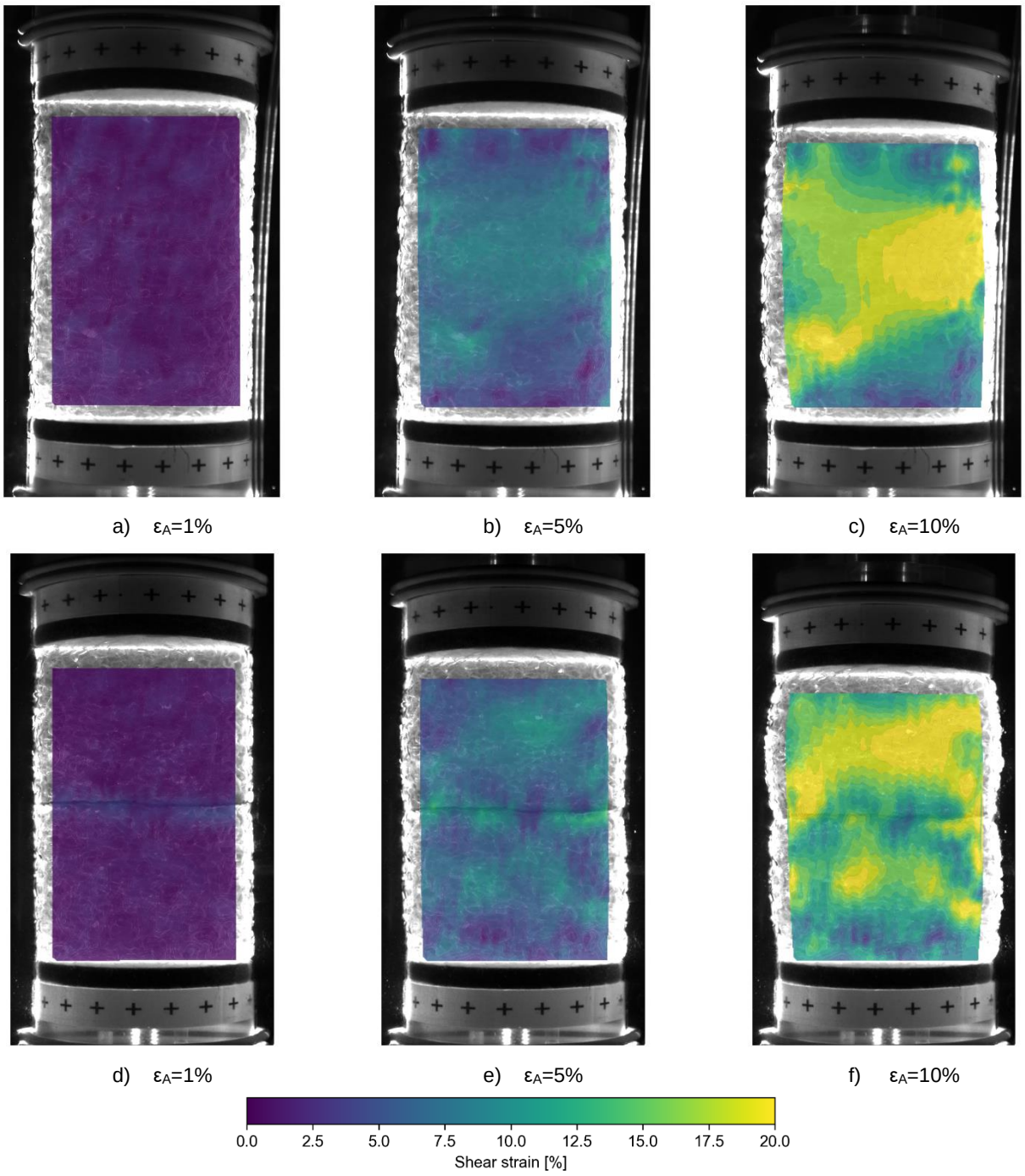

Figure 4. Maximum, total shear strain in Unreinforced Sample 1(a-c) and Reinforced Sample 2 (d-f) for different levels of axial strain

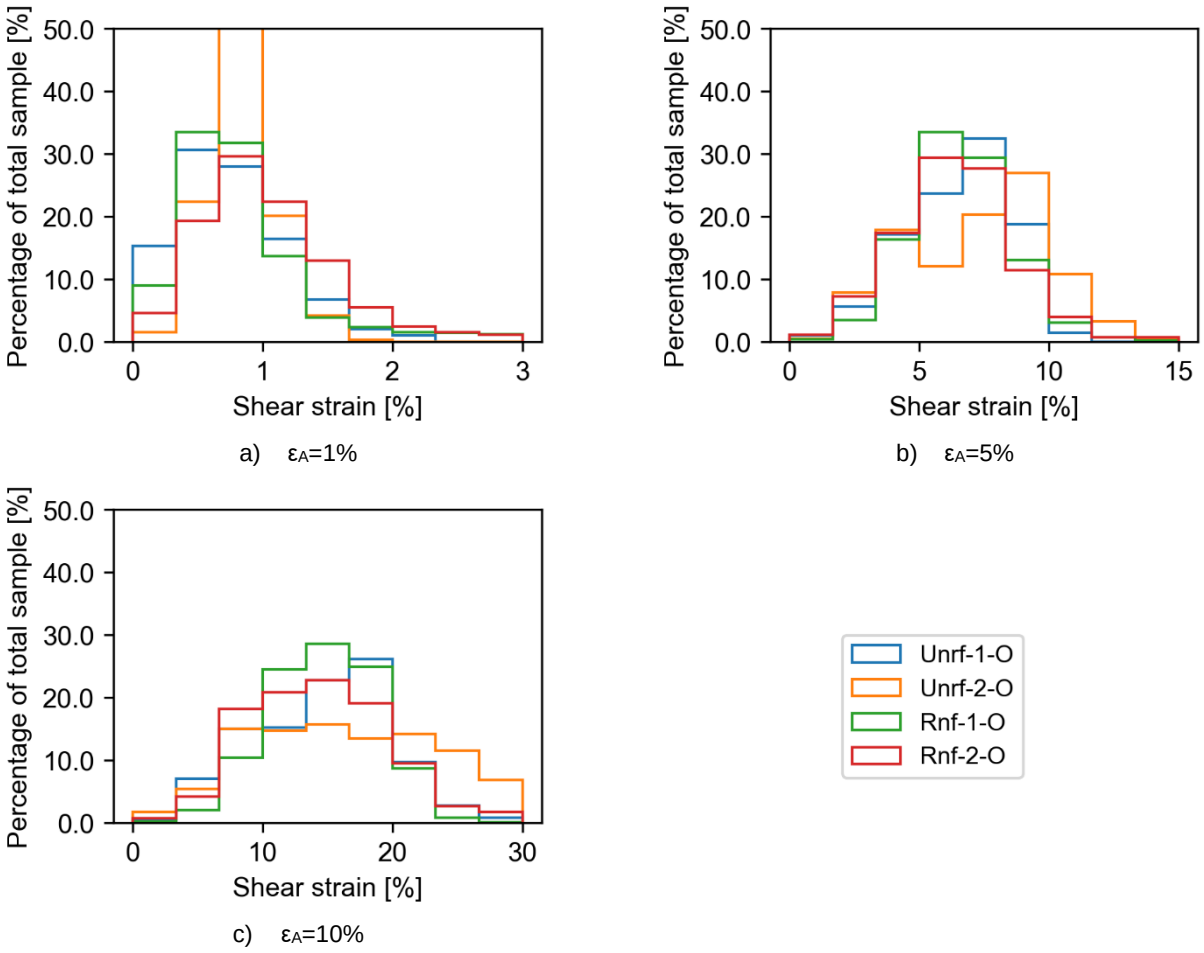

Figure 5. Histograms of the total shear strain distribution in the samples, at different axial strains

3.1 Effect of geotextile reinforcement on the strength of the sample.

In an unreinforced triaxial sample the inclination of the shear band is often considered to be $\theta = 45° + \phi/2$ as defined based on a Mohr's circle state of stresses. An alternative model considering non-associative flow was proposed by Roscoe (1970). According to this model, the angle of the shear band equals $\theta = 45° + \psi/2$. Kawamoto et al. (2018) found the model by Roscoe to be a better fit to shear bands observed from X-ray tomography images of a triaxial test on sand.

The average angle of dilation measured for the single sized quartz used in this study was 13.5°, thus a shear band inclination of 51.7° is expected for an unreinforced sample. For the reinforced samples the shear band was forced to the top half of the sample (see the shear bands in Figures 4c, 6e & 6f), equivalent to a shear band inclination of 45°. Considering that the theoretical inclinations were derived for a continuum the difference between 45° and 51.7° is considered minor. As the inclination of the failure planes were similar, is it may be inferred that the deviatoric stress at failure was similar for the reinforced and unreinforced samples. This resulted in similar stress-strain responses (see Figure 2a) and strain distributions (see Figure 5) for the reinforced and unreinforced samples. Consequently, even though the presence of the geotextile resulted in local changes in the behavior of the sample (see Section 3.1), its influence on the global strength was not as pronounced as anticipated based on results previously reported in the literature.

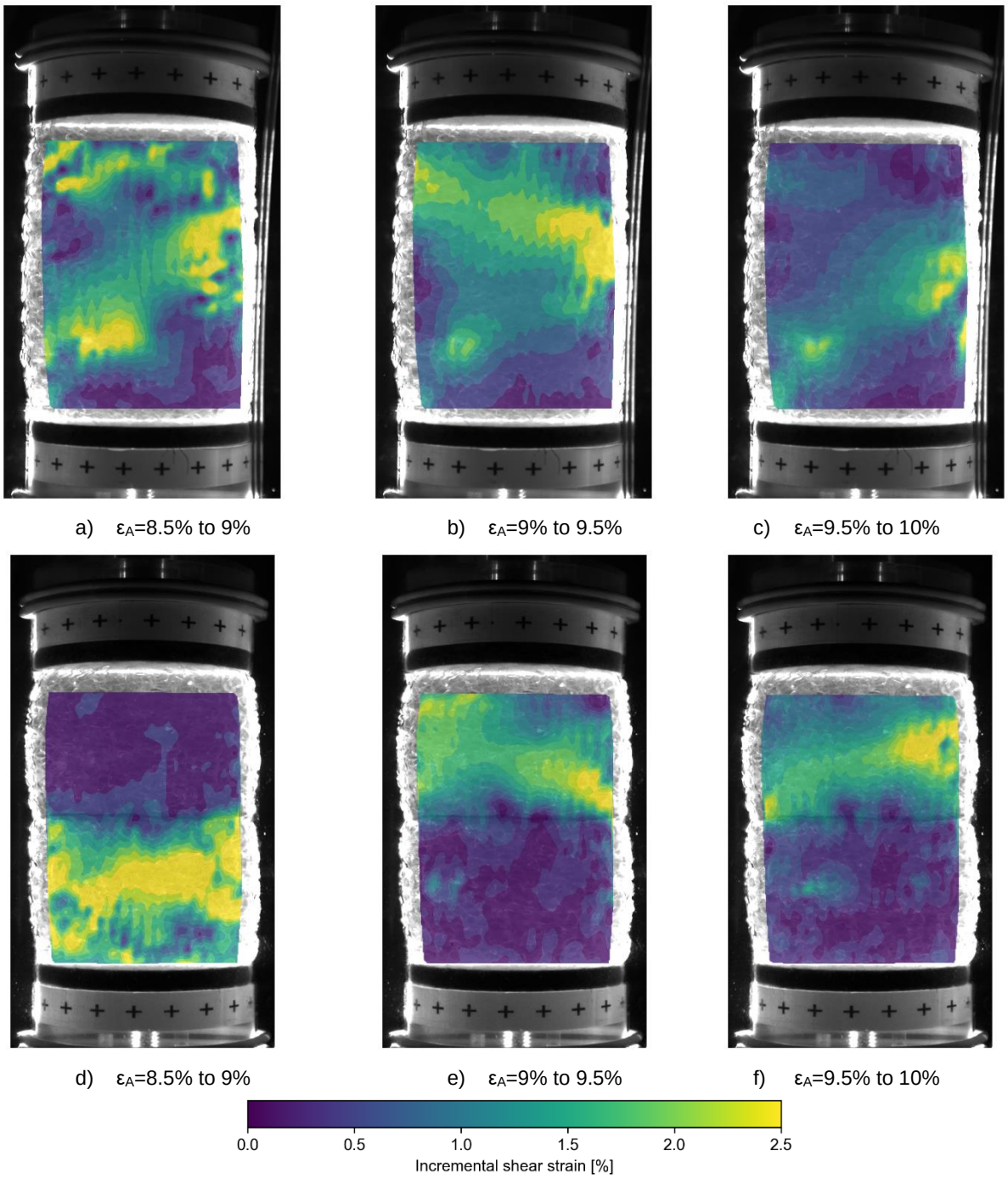

Figure 6. Incremental shear strain in the Unreinforced Sample 1(a-c) and Reinforced Sample 2 (d-f) for selected levels of axial strain

4. FINAL REMARKS

Triaxial tests were done two unreinforced and two geotextile reinforced samples of uniformly graded fused quartz. These samples were saturated with an oil with the same refractive index as the quartz to create a transparent media. By considering the distribution of shear strain through the samples, it was found that the geotextile resulted in the quartz

above and below the sample shearing independently. The region of particles actively failing continuously varied as the test progressed and was found to be a function of the axial strain increment under consideration.

By considering the radial strain that developed in the samples, as well as the angle of dilation, it was found that the geotextile provided some lateral restraint to the quartz. However, the effect of the geotextile on the overall strength of the sample was not as pronounced as expected from literature. These results are specific to a uniformly graded, fused quartz tested at ~190 kPa confinement. Further research is required to investigate the effect of different gradings, as well as confining pressures, on the shear band formation in geotextile reinforced samples.

ACKNOWLEDGEMENTS

The financial assistance of Tensar International Corporation for this study is acknowledged by the authors. Opinions expressed and conclusions presented are those of the authors and are not necessarily to be attributed to Tensar International Corporation.

4.1 REFERENCES

Amirpour Harehdasht, S., Karray, M., Hussien, M.N., Chekired, M. (2017). Influence of Particle Size and Gradation on the Stress-Dilatancy Behavior of Granular Materials during Drained Triaxial Compression. *International Journal of Geomechanics 17*

Ezzein, F.M., Bathurst, R.J. (2011). A Transparent Sand for Geotechnical Laboratory Modeling. *Geotechnical Testing Journal 36*: 590-601.

Frydman, S., Zeitlen, J.G., Alpan, I. (1973). The Membrane Effect in Triaxial Testing of Granular Soils. *Journal of Testing and Evaluation 1*:37–41.

Goodarzi, S., Shahnazari, H. (2019). Strength enhancement of geotextile-reinforced carbonate sand. *Geotextiles and Geomembranes* 47:128–139.

Guo, P., Xu, X. (2007). Shear strength, interparticle locking, and dilatancy of granular materials. *Canadian Geotechnical Journal* 44: 579–591.

Haeri, S.M., Noorzad, R., Oskoorouchi, A.M. (2000). Effect of geotextile reinforcement on the mechanical behavior of sand. *Geotextiles and Geomembranes*:18, 385-402

Head, K.H. (2014). *Manual of soil laboratory testing*, 3rd ed., Whittles Publishing, Caithness, Scotland, U.K.

Kawamoto, R., Andò, E., Viggiani, G., Andrade, J.E., 2018. All you need is shape: Predicting shear banding in sand with LS-DEM. *Journal of the Mechanics and Physics of Solids* 111, 375–392.

Latha, M.G., Murthy, V.S. (2006). Investigations on Sand Reinforced with Different Geosynthetics. *Geotechnical Testing Journa*: 29: 474-481

Li, X.S., Dafalias, Y.F. (2000). Dilatancy for cohesionless soils. *Géotechnique* 50:449–460

Oda, M., Kazama, H. (1998). Microstructure of shear bands and its relation to the mechanisms of dilatancy and failure of dense granular soils. *Géotechnique* 48:465–481.

Ozbay, A., Cabalar, A.F. (2016). Effects of triaxial confining pressure and strain rate on stick-slip behavior of a dry granular material. *Granular Matter* 18.

Palmeira, E.M. (2009). Soil–geosynthetic interaction: Modelling and analysis. *Geotextiles and Geomembranes* 27:368–390.

Peng, X., and J. G. Zornberg. (2017). Evaluation of load transfer in geogrids for base stabilization using transparent soil. *Transportation Geotechnics and Geoecology*. Elsevier, Saint Petersburg, Russia: 307-314.

Stanier, S.A., Blaber, J., Take, W.A., White, D.J. (2016). Improved image-based deformation measurement for geotechnical applications. *Canadian Geotechnical Journal* 53:727–739.